



An acoustic levitator design for suspending cosmic dust analogues and aerosol particles in light scattering experiments

A. Colin^{1,2} · O. Muñoz¹ · F. J. García-Izquierdo¹ · E. Frattin¹ · J. Martikainen¹ · Z. Gray^{1,3} · J. L. Ramos¹ · J. Jiménez¹ · A. Tobaruela¹ · J. M. Gómez-López¹ · I. Bustamante¹ · J. C. Gómez¹ · F. Moreno¹ · A. Marzo⁴

Received: 29 November 2024 / Accepted: 28 March 2025
© The Author(s) 2025

Abstract

We present a design of an acoustic levitator composed of 35 ultrasonic transducers operating at 40 kHz configured to form a spherical cavity. The acoustic radiation force measured experimentally in the center of the cavity is $F_{rad} \approx 9.6mN$, enough for levitating spheres as well as irregular particles of different materials of up to ~50 mg. Levitation tests have been performed with particles of different geometries and compositions, including liquid droplets and minerals relevant in studies of atmospheric aerosol and cosmic dust. This device has been deployed in the center of a polar nephelometer set-up to conduct studies of light scattering by irregular solid particles and liquid droplets. Test experiments have been carried out using a 1.5 mm diameter NBK-7 glass sphere, for which three elements of the scattering matrix have been measured as functions of the scattering angle using a 647 nm diode laser. Mie theory calculations of the scattering matrix elements at this wavelength agree well with the measurements, demonstrating the functionality of the whole device.

Keywords Acoustic levitator · Ultrasonic transducer · Cosmic dust · Light scattering · Irregular particles

✉ A. Colin
angelenrique.sanchez@uca.es

¹ Instituto de Astrofísica de Andalucía, Glorieta de la astronomía S/N, 18008 Granada, Spain

² Universidad de Cádiz, República Saharhui, 12, 11519 Puerto Real, Cádiz, Spain

³ Department of Physics, University of Helsinki, Gustaf Hällströmin Katu 2, P.O. Box 64, 00014 Helsinki, Finland

⁴ Universidad Pública de Navarra, Campus de Arrosadía, 31006 Pamplona, Spain

1 Introduction

The first studies of acoustic levitation in the XIX century aimed at measuring the speed of sound and visualizing longitudinal standing waves by means microparticles of fine dust in a transparent tube [14]. Since then, several theories have been developed to describe this phenomenon and find new specific applications [10, 13, 23, 27]. With the rise of miniaturized technologies, the use of acoustic levitators is becoming increasingly popular because of the availability of commercial ultrasonic transducers at very low cost. This brings up many opportunities, not only for researchers, but also for educational purposes.

In general terms, an acoustic levitator can be built with a transducer using: a) a plane reflector, b) a concave reflector or c) another transducer at the same frequency placed in the opposite position. In any case, the levitator needs to be connected to a signal generator producing sinusoidal standing acoustic waves. The device can be designed in such a way that the acoustic radiation force exerted on a particle situated between the two ‘loudspeakers’ is enough to levitate it. Such devices are useful in many research fields, particularly in those where contactless manipulation of samples is needed. In biology for example, acoustic levitation is used for harmless manipulation of small living animals [1, 26]. In medicine, this technique is being explored to manipulate single drops of human blood to enable the diagnosis of blood diseases [5]. In materials science, levitation experiments are conducted to study physical effects under microgravity conditions [24]. Today, new developments of levitators allow controlling transportation and orientation of samples in any direction while they are levitating in the midair [15, 16].

The Cosmic Dust Laboratory (CoDuLab) at the Instituto de Astrofísica de Andalucía (IAA), in Granada, Spain, is an experimental facility devoted to the characterization of the light scattering properties of cosmic dust analogues samples [20]. The goal is to get insight on the physical properties (size, composition and morphology) of cosmic dust grains by the analysis of their measured scattering matrices as functions of the scattering angle [12, 19]. To date, the scattering matrices of clouds of randomly oriented micron-sized dust particles have been measured by placing at the instrument target region an aerosol stream produced by a so-called aerosol generator. The aerosol generator can handle particles with radii ranging from below the micron up to a maximum radius of 100 microns. The acoustic levitator presented here aims at extending the size range of the solid particles that can be analyzed at CoDuLab up to a few millimeters. Also, the capability of manipulating liquid droplets enables scattering experiments devoted to characterizing liquid samples where the droplets may act as a convenient enclosure of smaller particles. This may prove useful in exploring the potential of light scattering in the diagnosis of certain medical diseases in body fluids.

In this paper we present a design of an acoustic levitator composed by 35 ultrasonic transducers operating at a frequency of 40 kHz configured in a spherical geometry of diameter 8λ , where $\lambda \approx 8.6$ mm is the wavelength of the standing

wave at 20 °C. This design is based on the technical principles of a previous levitator called ‘TinyLev’ [17], and has been implemented according to the requirements of CoDuLab. This paper is organized as follows: Sect. 2 summarizes the theory of acoustic levitation. In Sect. 3 the development of the levitator design is described. Section 4 describes the control-electronics and the control software interface. The experimental results are presented in Sect. 5, it includes measurements of the acoustic force exerted by three different configurations of ultrasonic transducers. The light scattering technique and optimization method of the CoDuLab apparatus are explained in Sect. 6, in which we present light scattering measurements of a levitated NBK-7 glass sphere characterized from Edmund Optics ($\varnothing 1.5\text{ mm} \pm 0.0025\text{ mm}$). Finally, the conclusions and future application are included in Sect. 7.

2 Theory

Important efforts have been invested in extending the acoustic levitation theory to different resonant geometries [6, 8], and even more to achieve a second-order approximation for ultrasound perturbations in fluids [7]. Nevertheless, the first-order approximation is enough for the development of this work. Here, we follow the analysis stated by Andrade et al. [3] assuming a small rigid sphere of radius $R \ll \lambda$ immersed in an ideal fluid. According to this analysis in the simplest formulation of a standing wave field, a single-axis acoustic levitator consists of a transducer and a plane-reflector separated conveniently by a distance of a multiple of the half-wavelength associated to the ultrasonic emission. Thus, a resonant cavity of length $L \approx n \lambda/2$ is formed, where λ is the wavelength of the standing wave. The first operation mode in such levitator occurs when $L \approx \lambda/2$, where only one node position at $z = \lambda/4$ exists. Therefore, in a cavity of length L , the n^{th} node position will be $z_n = n \lambda/2 + \lambda/4$, with $n = 0, 1, 2, 3 \dots$

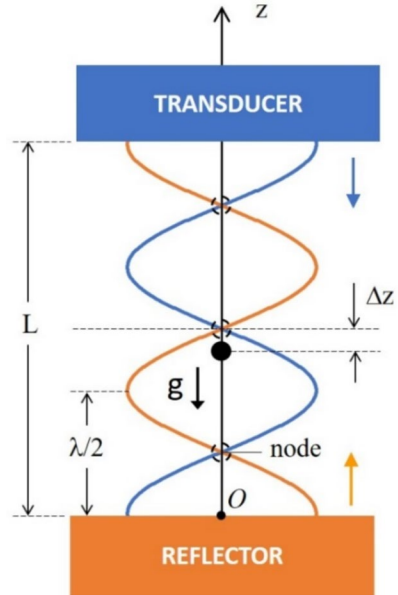
A very light object much smaller than λ should levitate in any node where the acoustic pressure is zero, whereas for heavier objects its levitation position will be slightly below of such node due to the action of gravity, as is depicted schematically in Fig. 1.

The acoustic radiation force F_{rad} exerted on a levitated sphere of density ρ_p , and the minimum acoustic pressure amplitude p_0^{min} , required to levitate such sphere are given respectively by:

$$p_0^{min} = \sqrt{\frac{6\rho_0 c_0^2 m g}{5\pi R^3 k}} = \sqrt{\frac{8\rho_0 \rho_p c_0^2 g}{5k}} \tag{1}$$

$$F_{rad} = \frac{5\pi R^3 k p_0^2}{6\rho_0 c_0^2} \sin(2kz) \mathbf{k} \tag{2}$$

Fig. 1 Sketch of the acoustic levitation of a sphere placed at the node in the middle of the resonant cavity (based in Fig. 2 of [3])



where ρ_0 is the fluid density, c_0 is the speed of sound in such fluid, p_0 is the acoustic pressure amplitude, z is the vertical position of the sphere; g is the acceleration of gravity, m is the mass of the sphere, and $k = 2\pi/\lambda = \omega/c_0$ is the wave number ($\lambda = c_0/f$ and $f = \omega/2\pi$ are respectively the wavelength and frequency of the standing wave).

In the presence of gravity, the gravity force $\mathbf{F}_g = -mg\mathbf{k}$ acts all time on the sphere, hence the levitation is possible only when $F_{rad} > F_g$. The vertical displacement of the sphere from the node is proportional to the radiation force, hence F_{rad} can also be approximated by Eq. (3) as the restoring force of a spring:

$$\mathbf{F}_{rad} = -K(z - z_n)\mathbf{k} \tag{3}$$

where the elastic constant is given by:

$$K = \frac{5\pi R^3 k^2 p_0^2}{3\rho_0 c_0^2} \tag{4}$$

In Eq. (4) we can use $k = 2\pi f/c_0$ to obtain:

$$p_0 = \sqrt{\frac{3K\rho_0 c_0^4}{5\pi R^3 (2\pi f)^2}} \tag{5}$$

It is important to keep in mind that the force that acts like a spring push the sphere towards the node. This analogy allows to calculate the distance between the sphere and the node by:

$$\Delta z = z_n - z = \frac{mg}{K} = \frac{4\rho_0\rho_p c_0^2 g}{5k^2 p_0^2} \quad (6)$$

When the sphere is perturbed by an external force, its movement is similar to that of a simple oscillator whose natural oscillation frequency can be estimated by:

$$\Omega = \sqrt{\frac{K}{m}} = \sqrt{\frac{5k^2 p_0^2}{4\rho_0\rho_p c_0^2}} \quad (7)$$

The natural oscillation frequency Ω is proportional to the acoustic pressure amplitude and can be controlled by varying the pressure amplitude in the cavity.

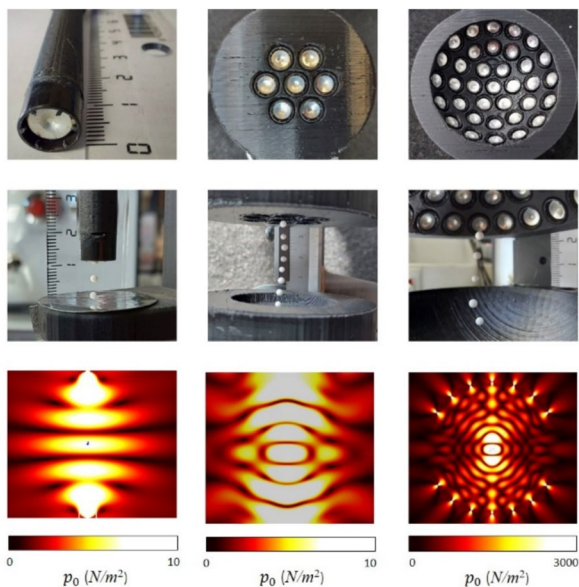
3 Levitator design

Our ultimate goal is to levitate a range of materials that spans from fluids to mineral particles of varied sizes and porosity. The following strategy has been followed for the design of the levitator. We started with the simplest model that has been gradually refined through different stages to achieve a design that allows us to levitate a broader range of materials while maintaining maximum levitation stability. The simplest model consists of a single element transducer. This compact device has diameter of 1 *cm* and a length of 10 *cm* and a power consumption smaller than 1 *W* (Fig. 2. left). It consists of a reflector plane in the third resonant mode and a single cavity of physical length $L \approx 3\lambda/2$, where $\lambda \approx 8.6$ *mm*. We started with this simple initial model to verify the validity of the theory. Additionally, it allows us to use it in training and outreach activities. In a second step we developed a 7-element in a circular array device that allows to levitate several samples simultaneously (Fig. 2. middle). Here, the samples can be placed in the generated nodes by each transducer. The area covered with this array is around 3 *cm* in diameter. This device operates with a reflector plane in a whole cavity of $L \approx 4\lambda$, thus providing eight operation modes for each transducer. Its whole power consumption is less than 3 *W*. Both devices are limited to irregular samples with very low density and very small liquid droplets.

To levitate higher-density samples we increased the array up to 35-elements configured to form a hemispherical geometry of radius $R \approx 4\lambda$ (Fig. 2. right). A concave reflector with the same radius of curvature is placed opposite to the transmitter. The roughness of the concave surface is ~ 50 μm , achieved manually by using sandpaper of different grain sizes. The surface was then coated with a thin layer of black paint of high opacity. Both parts are separated vertically by 24 *mm*. The transmitter is capped to prevent manual contact with the electrical connections. This design allows us to levitate particles of up to 50 *mg* located in the center of the spherical cavity where the maximum value of the acoustic force is exerted. The whole power consumption of this device is around 11 *W*.

In all three designs, we used ultrasonic transducers (MANORSHI, model: MSO-P1040H07 TR) operating at 40 *kHz* mounted on 3D printed mounts. In order to

Fig. 2 Array configurations and operation modes with simulations of acoustic fields: 1-element (left), 7-elements (middle), and 35-elements in a spherical cavity of $R=4\lambda$ (right)



have clean emission from all transducers, we removed their protection grids from its plastic case because in this way we observed that the signal amplitude could be increased up to $\sim 10\%$.

With these designs we levitated spheres of expanded polystyrene (EPS) of ~ 2 mm in diameter. The very low density of this material allows trapping the spheres in each node of the acoustic field; its vertical displacement caused by gravity could be considered as negligible. Figure 2 shows the three configurations with their operative modes, and acoustic field simulations made with the ‘Ultraino package’ (<https://github.com/asiermarzo/Ultraino>).

All structural components including the support were built with a 3D printer at 99% density and can be attached to each other by means of screws. The whole device is mounted on a metric XYZ-Positioner, which in turn is mounted on a 360° Rotary positioner (Edmund Scientific). Figure 3 shows the schematic design and a picture of the levitator mounted on the CoDuLab’s optical bench. In this picture we can appreciate the NBK-7 sphere levitating on the center of the cavity, which is illuminated with a 647 nm diode laser.

4 Control interface

The control interface shown in Fig. 4 (left panel) was developed particularly for this hardware and offers the following features:

- It contains a universal serial bus (USB) command handler that links the hardware control with the software located inside the laboratory control room. The next points describe the items controlled by this connection.

- Through digital outputs we can act on the phase control signals implemented in Tinylev, increasing or decreasing this gap. Similarly, it allows the activation of a reset signal to put them in phase.
- Through digital outputs, the power stage in each phase provided to the transducer array can be activated/deactivated.
- The power stage thermal control includes a dual full-bridge L298P driver (ST Microelectronics) with a junction-to-ambient thermal resistance of $13\text{ }^{\circ}\text{C/W}$, including its corresponding thermal dissipation pad. In this way, we achieve high stability of the output power, independent of temperature fluctuations, which will provide greater levitation stability over extended periods of time. The firmware cyclically reads a PT1000 temperature sensor every second and according to a programmed set point (40°) and a permissible hysteresis (10°), it automatically activates a fan installed on the L298P device.
- The temperature sensor reading is always available upon request from the software (Driver Temperature display, Fig. 5, left panel).
- The firmware automatic thermal control can be activated/deactivated from the software. In case this automatic control is deactivated, the software can activate/deactivate the fan upon user request.

The control software is a graphical user interface (GUI) environment that allows the user to interact with the levitator. This software is installed in the CoDuLab general control computer. Some of its features have been described above but, in addition, the following can be highlighted:

- Sample-position control (Fig. 4, left panel). From the main screen of the application the user can access to a continuous button to move the sample up (UP button) or down (DOWN button) with uniform speed. Likewise, the user has access to a button that generates a discrete movement, designed to shift the sample in or out of the measurement spot (UP pulse, Down pulse buttons). The Reset button turns

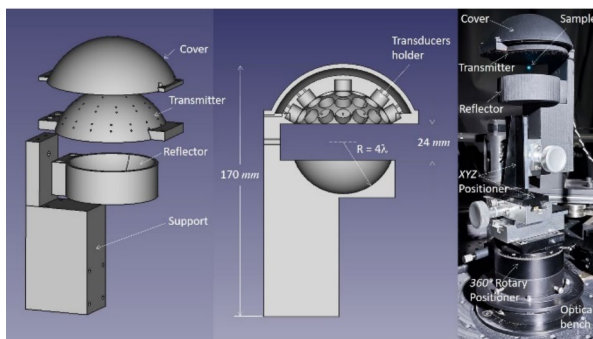
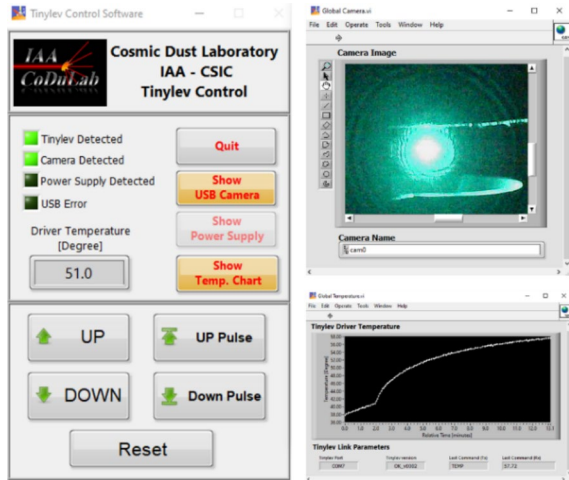


Fig. 3 Schematic design (not to scale) and a picture of the levitator mounted on the optical bench at CoDuLab

Fig. 4 Multi-windows software interface for the levitator's control with a plot of temperature and an image of the levitated sample during its characterization at CoDuLab

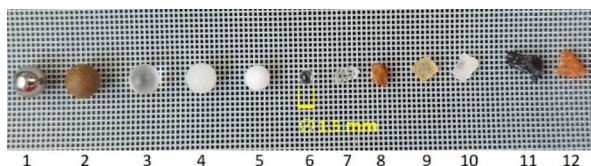


off the transceivers signal causing the levitated sample to settle in the levitator lower cup.

- Image of the low light vision camera (Fig. 4, top right panel). This camera allows the user to check if the sample to be analyzed is located in the path of the laser. It does not allow discriminating whether it is at the center of the beam, because when entering the measurement spot the image can become saturated. The user can present or close the presented image in a new window of the program, and also can select the image area of interest.
- Power driver temperature (Fig. 4, bottom right panel). The GUI continuously presents the current temperature of the power driver. It is marked with a red frame; in case the firmware has activated the extra dissipation fan in its automatic control cycle. Similarly, the user can review the history of the driver thermal behavior since the session was started, activating a window with a data graph.

The general goal of this software is to consume little resources from the operative system and not interfering with the laboratory control program, which is priority. For this reason, a multi-window platform was set for camera; power supply and thermal history control (see Fig. 4). The user shall only activate/deactivate the graphic processes required at all times.

Fig. 5 Spheres and irregular samples of different materials. The size of the fused quartz sphere is indicated in yellow (ϕ 1.5mm)



5 Experiment

5.1 Samples

The functionality of our levitator was tested with the levitation of a water droplet, 6 spheres and 6 irregular samples of different materials. The particles can be described referring to Fig. 5 as: metallic sphere (#1), silica gel sphere (#2), glass sphere (#3), polypropylene sphere (#4), polystyrene sphere (#5), fused quartz sphere (#6), quartz crystal (#7), ferruginous quartz crystal (#8), brown sugar (#9), sea salt (#10), volcanic ash (#11) and baked clay (#12). The physical properties of all samples are listed in Table 1.

For estimating the density ρ_p of each sample, in particular for the irregular samples, we used their physical dimensions to form a hypothetical geometrical solid, then we approximated its volume to obtain

$$\rho_p \approx \rho_p^{est} = \frac{m_{meas}}{V_{approx}} \quad (8)$$

where ρ_p^{est} is the estimated density; m_{meas} is the measured mass, and V_{approx} is the approximated volume.

The mass of all samples were measured using a microbalance (ADAM-Highland, model: HCB123) with a resolution of 1 mg. To ensure its performance, we used the plastic draft shield that surrounds the stainless-steel pan to avoid air perturbations and get more stable readings. For each reading we turned-on and turned-off the power supply during three times then we averaged its value.

5.2 Acoustic force measurements

For estimating the acoustic pressure amplitude p_0 in each of our designs, we measured first, the exerting acoustic force F_{meas} on the metallic pan of the microbalance. For this, we turned the reading mode of the microbalance to mN units. Then we placed each device in operative mode aligned to the center of the metallic pan, which in turn acts as a plane reflector isolated by the plastic draft shield. For each measurement, we varied manually the vertical distance from 0 to 4λ in $\lambda/2$ steps with respect to the reflector. For this, we used a metric XYZ-Axis positioner mounted on a 360° rotary positioner (Edmund Scientific), as is shown in Fig. 6.

For each reading we turned-on and turned-off the power supply during three times then we averaged its value. We observed that a single-element transducer generated ~ 1 W of power consumption and exerted a maximum acoustic force of ~ 0.36 mN on the reflector, whereas for the configuration of 7-elements, the power consumption and acoustic force were ~ 3 W and ~ 2.45 mN. For the arrangement with 35-element, those values were ~ 11.5 W and ~ 9.6 mN, respectively.

The plots in Fig. 7 summarize the acoustic force measured against vertical distance. Note that, for the spherical configuration, the variation of vertical distance every $\lambda/2$ step started around the center of the cavity, where its maximum value is

Table 1 Estimation of acoustic-levitation parameters for different materials

Sample	Material	Dimensions (mm)	Mass (mg)	Volume (mm ³)	ρ_p (kg/m ³)	F_g (mN)	Ω (Hz)	K (N/m)	Δz (mm)	P_0^{min} (N/m ²)	F_{rad} (mN)
1	Metallic	$\phi 3$	129	14.14	9125	1.26	70	0.624	2.03	5250	0.427
2	Silica gel	$\phi 3.4$	44	20.58	2138	0.431	144	0.908	0.47	2542	0.622
3	Glass	$\phi 3$	37	14.14	2617	0.363	130	0.625	0.58	2812	0.427
4	Polypropylene	$\phi 3$	19	14.14	1344	0.186	181	0.624	0.30	2015	0.427
5	Polystyrene	$\phi 2.4$	0.2	7.24	28	0.00196	1264	0.319	0.006	289	0.218
6	Fused quartz	$\phi 1.5$	5	1.77	2829	0.049	125	0.078	0.63	2924	0.0534
7	Quartz crystal	$\sim (2 \times 1.5 \times 1.2)$	4	~ 3.6	1111	0.039	-	-	-	1832	-
8	Fe Quartz crystal	$\sim (2 \times 1.5 \times 1.5)$	6	~ 4.5	1333	0.059	-	-	-	2007	-
9	Brown sugar	$\sim (2 \times 2 \times 1)$	5	~ 4	1250	0.049	-	-	-	1943	-
10	Sea salt	$\sim (2.5 \times 2 \times 1)$	8	~ 5	1600	0.078	-	-	-	2199	-
11	Volcanic ash	$\sim (4 \times 2 \times 1.5)$	10	~ 12	833	0.098	-	-	-	1587	-
12	Baked clay	$\sim (3 \times 2 \times 1)$	7	~ 3	2333	0.069	-	-	-	2655	-
13	Water	$\phi = 2$	4.19	4.19	1000	0.041	210	0.185	0.22	1738	0.127

expected. The maximum for the array of 7-elements occurred at a vertical distance of λ , whereas for a single element was at $3\lambda/2$.

The acoustic pressure amplitude, estimated for each device may be considered equivalent to:

$$p_o^{est} = \frac{F_{meas}}{A} \approx p_0 \tag{9}$$

where A is the area covered by the number of transducers in each case. As an example, each transducer has an emitter of $\sim 8\text{ mm}$ in diameter. Then, for a single transducer, $A = \pi r^2 \approx 5 \cdot 5^{-5} m^2$, therefore $p_o^{est} \approx 7.16 Nm^{-2}$. For the array of 7-elements, $A \approx 3.5 \cdot 5^{-4} m^2$ and $p_o^{est} \approx 6.96 Nm^{-2}$. For the hemispherical configuration whether we assume that the acoustic pressure converges to a point at the center of the cavity, it will tend to produce an indetermination in Eq. (9). To avoid this indetermination, we must consider a small area on the metallic plane reflector as a circumference of radius $r \neq 0$. Assuming for instance $r = 1\text{ mm}$, we obtain $A \approx 3.14 \cdot 5^{-6} m^2$, and therefore $p_o^{est} \approx 3056 \frac{N}{m^2}$.

If p_0 or Ω were known, the acoustic radiation force F_{rad} and the elastic constant K could be estimated easily by applying Eq. (2) or Eq. (3). However, experimentally their determination it is not a simple task. One of the most used experimental methods consists in using a laser vibrometer to obtain the pressure profile in the acoustic cavity, and by using a high-speed camera to capture the natural oscillatory movement of the sample, then plotting its vertical position as a function of time [2, 18]. In both cases, the data can be treated by graphical analysis. This method could not be used in in this work due to budgetary constraints. To address this issue, we considered that for each one of the levitated samples $p_0^{min} < p_o^{est}$ as is shown in Table 1. Ignoring sample #1 in this table, we observed that the highest estimated value of p_0^{min} corresponds to sample 6, which is slightly lower compared to p_o^{est} . Therefore, we can assume that $p_0 \approx p_0^{est}$ can be used for estimating K , Δz , Ω , and F_{rad} of each sphere. For the irregular samples it is not possible to do these estimations because of it is required the factor of dependence R .

We have discarded sample #1 in this assumption because its high density and weight requires at least $p_0^{min} \geq 5250 Nm^{-2}$ to be levitated. This value is

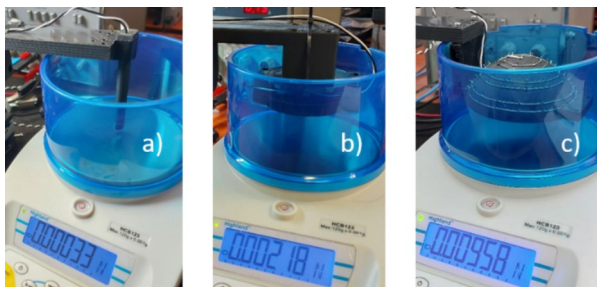
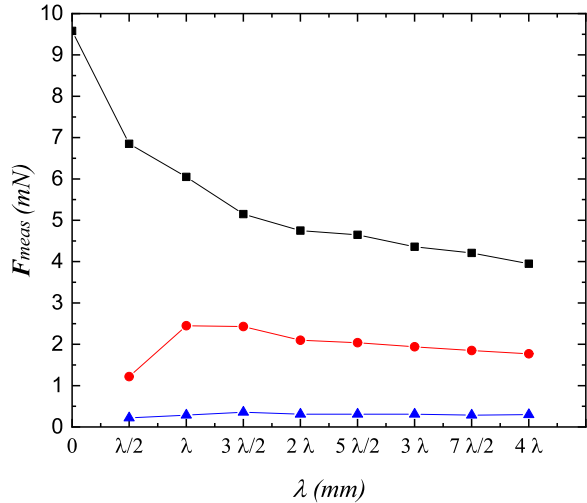


Fig. 6 Set-up for measuring the acoustic force with an electronic microbalance. a) a single element. b) 7-elements in a circular array. c) 35-elements in a hemispherical array

Fig. 7 Acoustic force against vertical distance ($\lambda \approx 8.6 \text{ mm}$) measured on the center of the microbalance. In blue: a single transducer; In red: 7-elements in circular array; In black: 35-elements in a hemispherical array



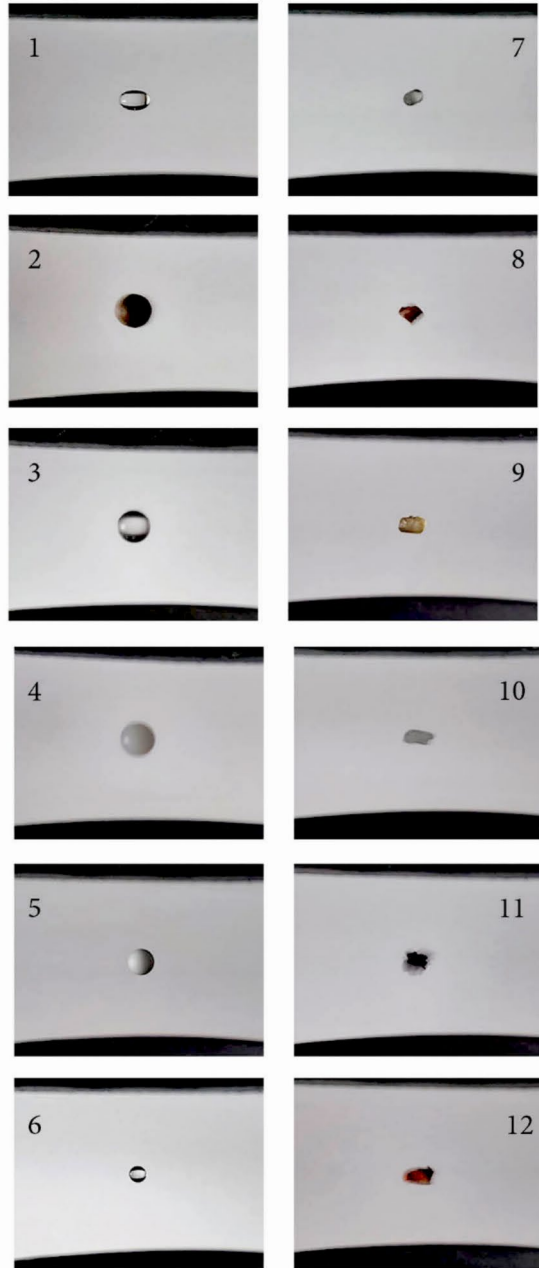
higher than the maximum value estimated for our levitator ($p_o^{est} \approx 3056 \text{ Nm}^{-2}$). For this reason, we levitated a water droplet instead (Fig. 8, number 1). The volume of the water drop was $\sim 5 \mu\text{l}$ filled with a syringe (Hamilton 65RN 5 μl). There are several studies in the literature related to liquid droplets levitation [9, 22], but our interest here for the moment was only for functionality tests and demonstrative purposes of our levitator. Interested readers can refer for example to an extended and practical study for acoustic levitation of water droplets [4].

5.3 Levitation tests

Figure 8 shows pictures of the samples taken during their levitation inside the spherical cavity of the levitator. In picture number 1 we can appreciate how the water droplet turns to an ovoid form, as expected for most of the levitated liquids. We observed that samples 2–4 could not be stabilized by varying the acoustic pressure amplitude in the cavity, but they remained levitating for long periods of time under constant oscillations as can be appreciated in their pictures. That may be due to the diameter size of these samples is quite bigger than $\lambda/2$, thus giving big volumes, and/or because their density p_o^{est} is close to p_o^{min} . In contrast, samples 5 and 6 remained stables and levitating during long periods of time (several hours).

On the other hand, the morphology of samples 7, 9 and 10 generated slow rotations around z -axis in both, right and left directions. The morphology of samples 8 and 11 caused very fast rotations thus turning the samples as solids of revolution, whereas sample 12 caused constant oscillations, as can be appreciated in their corresponding pictures.

Fig. 8 Pictures of the samples taken during their levitation on the spherical cavity of our levitator. Note that sample 1, the metallic sphere, was replaced by a water droplet of $5 \mu l$



The particular case of sample 5 (sphere of polystyrene), whose very low density turns that the levitator can be operative only with a few V_{pp} (volts-peak-to-peak). This sample could be levitated and stabilized for very long periods of time without appreciation of any change. Even more, this sample and of course other samples

with similar size and densities can be levitated using only one transducer, as was demonstrated in Sect. 3.

6 Light scattering apparatus

6.1 Description

CoDuLab is essentially a polar nephelometer designed to measure the angular dependence of the scattering matrix of cosmic dust analogue samples (Fig. 9). The 4×4 scattering matrix F of a particulate sample depends on the sample physical properties (such as size, morphology and composition), wavelength of the incident radiation, distance to the detector, and the scattering direction, which, for randomly oriented particles, is fully described by the scattering angle θ . The origin of the coordinate system is located inside the illuminated particle. In this coordinate system, the scattering angle is defined as the angle between the incidence and scattering directions. The plane of reference is the scattering plane, i.e., the plane containing the incident and the scattered light. This scattering matrix acts on the Stokes vector of the incident light beam, which defines its flux and its linear and circular polarization states, modifying the Stokes vector of the scattered light accordingly [11]. The set-up of the light scattering apparatus at CoDuLab has been described before in [19, 20], and therefore only a brief description is provided here. Light from a diode laser (available wavelengths are 405, 488, 514 and 647 nm) passes through a polarizer and an electro-optic modulator before hitting a sample placed at the center of the set-up. The sample can be a thin cloud of micron-sized particles generated by an aerosol generator (solid particles) or a nebulizer (liquid droplets). The aim of this work is to position a *mm*-sized single cosmic dust grain at the center of the scattering volume (the origin of our reference coordinate system) for a long enough time to perform the scattering measurements. The use of a levitator for sample positioning allows us to avoid the use of supports or containing vessels, whose reflections could distort

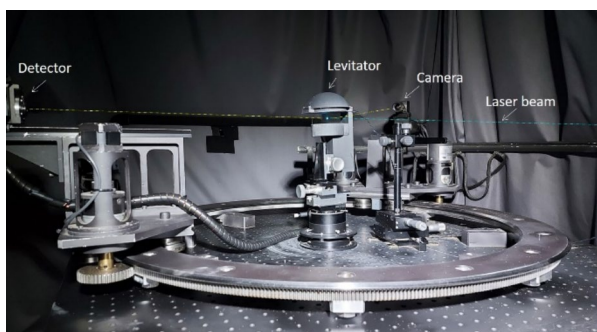


Fig. 9 Experimental set-up with the levitator implemented into the light scattering apparatus

the measurements. Furthermore, the use of the levitator facilitates the retrieval of the sample after the scattering measurements.

The light scattered by the sample is detected by two photomultipliers (detector and monitor). The detector moves around the center of a 1 m diameter ring spanning scattering angles (θ) between 3° and 177° . The monitor is placed at a fixed angular position and its mission is controlling the fluctuations of the laser signal and/or the sample. There are two optional optical elements in front of the detector (a quarter waveplate and an analyzer). The modulation of polarization of the incident light, in combination with the optional optical elements and lock-in amplification allow to simultaneously obtain several elements of the scattering matrix with a high signal to noise ratio. In particular, the element $F_{11}(\theta)$, known as the phase function, is proportional to the flux of the scattered light for unpolarized incident light. Also, for unpolarized incident light, the ratio $-F_{12}(\theta)/F_{11}(\theta)$ is called the degree of linear polarization (DLP).

Alignment and optimization are performed by measuring spherical particles, for which exact calculations of the scattering matrix can be performed using Mie theory, and hence a reference for the measurement quality is available. Usually, a nebulizer is employed to generate a cloud of micron-sized spherical water droplets. The alignment of the optics and the voltages applied to the optical modulator are fine-tuned until agreement between the measurements and the Mie model results are good [19].

6.2 Scattering matrix measurements

We have tested the performance of the nephelometer plus levitator by comparing measured scattering matrix elements of an NBK-7 glass sphere ($\phi = 1.5$ mm, refractive index $m = 1.5148 + i1.22E-08$) to results of Lorenz-Mie computations for the same sphere. The calibration sphere size has been selected similar to that of the potential target dust grains. The objective is to optimize the position of the sphere relative to the beam and detectors, as well as the beam spot size, and determining whether the stability of the position of the levitated particle is enough to perform the scattering measurements.

In Fig. 10, we display the measured (symbols) and computed (solid lines) elements and ratio of elements ($F_{11}(\theta)$, $-F_{12}(\theta)/F_{11}(\theta)$, and $F_{14}(\theta)/F_{11}(\theta)$) of the scattering matrix for the NBK-7 sphere. Measurements and computations are performed at a wavelength of 647 nm.

Measured data span over the 3° and 177° scattering angle range. We find a good agreement between the experimental and theoretical data across the entire range of scattering angles. This indicates a good alignment and homogeneous illumination of the sphere in the optical train. The $F_{14}(\theta)/F_{11}(\theta)$ ratio for a spherical particle is equal to zero at all scattering angle range. Small differences between computed and measured data are due to the reflection on the levitator reflector part of the light scattered by the transparent sphere. This stray light is minimum when dealing non-transparent irregular dust grains.

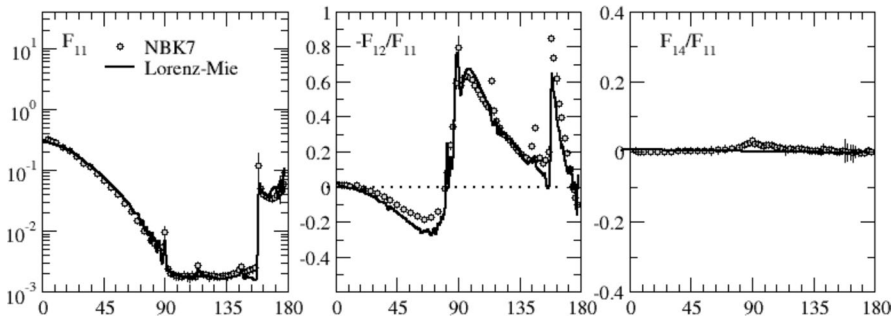


Fig. 10 Left: Phase function (F_{11}), middle: degree of linear polarization $-F_{12}/F_{11}$ and F_{14}/F_{11} for NBK7 glass sphere of $\varnothing = 1.5 \text{ mm}$ at 488 nm . Empty circles correspond to the experimental data. Solid lines correspond to Lorenz-Mie computations at 647 nm for a sphere with the same diameter, refractive index as the NBK-7 sphere. Experimental errors are presented by bars. When no error bar is shown is because it is smaller than the symbol

7 Conclusions and outlook

Light scattering experiments of large (*mm*-sized) dust samples require contactless manipulation to avoid interference of supporting pods and to enable easy measurement in random orientation. Acoustic levitation can be used for this purpose. We have presented the design of an acoustic levitator capable of levitating different types of samples with masses up to about 50 mg . Such design is easily re-scalable to a bigger one to levitate heavier samples just by increasing the radius of curvature of the cavity and the number of transducers.

Our simulations and levitation experiments demonstrate the functionality of our device. The scattering results obtained confirm that the acoustic levitator can be used to suspend samples in the optical train of CoDuLab's light scattering apparatus. This expands the range of samples that can be studied at CoDuLab, not only to large compact particles as those considered in this work, but also to low porosity aggregates that may be formed by levitating together a bunch of smaller particles. Large particles with high porosity are currently believed to be abundant in the cometary tail of comet 67P/Churyumov-Gerasimenko, and play a role in explaining remote and in situ photopolarimetric observations [21]. Being able to suspend *mm*-sized liquid droplets also means that light scattering photopolarimetry can now be tested at CoDuLab as medical diagnostic method using body fluids (e.g. blood).

Two approaches can be considered: levitation with full control over the particle's orientation [15], or levitation that allows chaotic rotation as is the case of our levitator. The first option enables the use of advanced numerical techniques to, for instance, determine the refractive index of the levitated particle with high precision [25], while the second allows us to simulate random orientation, as is the case in our experiment.

Acknowledgements This work has been funded by PID2021 -1233700B- 100/AEI/<https://doi.org/10.13039/501100011033/FEDER> and Severo Ochoa grant CEX2021 -001131-S funded by MCIN/AEI/<https://doi.org/10.13039/501100011033>.

Author contribution A.C. and O.M. wrote the main manuscript text. Z.G., J.C.G and F.M. prepared Figs. 9, 10. F.J.G.I, E.F., J.M. and I.B. prepared Figs. 2, 3, 9. J.L.R., J.J., A.T., and J.M.G.L. prepared text of Sect. 4 and Figs. 4. A.M. prepared Fig. 2, 4. All authors reviewed the manuscript.

Funding Funding for open access publishing: Universidad de Cádiz/CBUA.

Data availability No datasets were generated or analysed during the current study.

Declarations

Competing interests The authors declare no competing interests.

Open Access This article is licensed under a Creative Commons Attribution 4.0 International License, which permits use, sharing, adaptation, distribution and reproduction in any medium or format, as long as you give appropriate credit to the original author(s) and the source, provide a link to the Creative Commons licence, and indicate if changes were made. The images or other third party material in this article are included in the article's Creative Commons licence, unless indicated otherwise in a credit line to the material. If material is not included in the article's Creative Commons licence and your intended use is not permitted by statutory regulation or exceeds the permitted use, you will need to obtain permission directly from the copyright holder. To view a copy of this licence, visit <http://creativecommons.org/licenses/by/4.0/>.

References

1. Akkoyun, F., Gucluer, S., Oszcelik, A.: Potential of the acoustic micromanipulation technologies for biomedical research. *Biomicrofluidics* **15**, 061301 (2021). <https://doi.org/10.1063/5.0073596>
2. Andrade, M.A.B., Pérez, N., Adamowski, J.C.: Experimental study of the oscillation of spheres in an acoustic levitator. *J. Acoust. Soc. Am.* **136**(4), 1518–1529 (2014). <https://doi.org/10.1121/1.4893905>
3. Andrade, M.A.B., Pérez, N., Adamowsky, J.C.: Review of progress in acoustic levitation. *Braz. J. Phys.* **48**, 190–213 (2018). <https://doi.org/10.1007/s13538-017-0552-6>
4. Andrade, M.A.B., Marzo, Asier: Numerical and experimental investigation of the stability of a drop in a single-axis acoustic levitator. *Phys. Fluids* **31**, 117101 (2019). <https://doi.org/10.1063/1.5121728>
5. Ansari, V., Hosseninzadeh, C. Brugnara., Glynn Holt, R.: Shape oscillations of single blood drops: applications to human blood and sickle cell disease. *Sci Rep* **8**, 16794 (2018). <https://doi.org/10.1038/s41598-018-34600-7>
6. Barmatz, M., Collas, P.: Acoustic radiation potential on a sphere in plane, cylindrical and spherical standing wave fields. *J. Acoust. Soc. Am.* **77**(3), 928–945 (1985). <https://doi.org/10.1121/1.392061>
7. Bruus, H. *Acoustofluidics 7: the acoustic radiation force on small particles*. *Lab Chip*, **12**, 1014–1021 (2012). <https://doi.org/10.1039/C2LC21068A>
8. Collas, P., Barmatz, M., Shipley, C.: Acoustic levitation in the presence of gravity. *J. Acoust. Soc. Am.* **86**(2), 777–787 (1989). <https://doi.org/10.1121/1.398200>
9. Crum, L.A.: Acoustic force on a liquid droplet in an acoustic stationary wave. *J. Acoustic Soc. Am.* **50**(Part 2), 157–163 (1971). <https://doi.org/10.1121/1.1912614>
10. Gor'kov, L.P.: On the forces acting on a small particle in an acoustic field in an ideal fluid. *Sov. Phys. Dokl.* **6**, 773. Translated from *Dok. Akad. Nauk SSSR* **140**, 88 (1961).
11. Hovenier, J.W., van der Mee, C.V.M., Domke, H.: *Transfer of polarized light in planetary atmospheres: basic concepts and practical methods*. Kluwer, Dordrecht, NL (2004)

12. Hovenier, J.W., Muñoz, O.: Light scattering in the Solar System: An introductory review. *JQRSRT* **110**, 1280–1292 (2009). <https://doi.org/10.1016/j.jqsrt.2009.02.011>
13. King, L.V.: On the acoustic radiations pressure on spheres. *Proc. R. Soc. London Ser. A* **147**, 212–240 (1934). <https://doi.org/10.1098/rspa.1934.0215>
14. Kundt, A.: "Acoustic Experiments". The London, Edinburgh, and Dublin Philosophical Magazine and Journal of Science. Vol. 35, no. 4. UK: Taylor & Francis. pp. 41–48, (1868). <https://doi.org/10.1080/14786446808639937>
15. Maconi, G., Helander, P., Gritsevich, M., et al.: 4 π Scatterometer: A new technique for understanding the general and complete scattering properties of particulate media. *JQRSRT* **246**, 106910 (2020). <https://doi.org/10.1016/j.jqsrt.2020.106910>
16. Marzo, A., Seah, S.A., Drinkwater, B.W., et al.: Holographic acoustic elements for manipulation of levitated objects. *Nat. Commun.* **6**, 8661 (2015). <https://doi.org/10.1038/ncomms9661>
17. Marzo, A., Barnes, A., Drinkwater, B.W.: TinyLev: A multy-emitter single-axis acoustic levitator. *Rev. Sci. Instrum.* **88**, 085105 (2017). <https://doi.org/10.1063/1.4989995>
18. Mecham, R.D. Langevin transducer analysis and acoustic levitation. Senior thesis, Lake Forest University <<https://core.ac.uk/download/pdf/214314585.pdf>> (2018). Accessed 15/09/2024.
19. Muñoz, O., Moreno, F., Guirado, D., et al.: Experimental determination of scattering matrices of dust particles at visible wavelengths: The IAA light scattering apparatus. *JQRSRT* **111**, 187–196 (2010). <https://doi.org/10.1016/j.jqsrt.2009.06.011>
20. Muñoz, O., Moreno, F., Guirado, D., et al.: The IAA cosmic dust laboratory: Experimental scattering matrices of clay particles. *Icarus* **211**, 894–900 (2011). <https://doi.org/10.1016/j.icarus.2010.10.027>
21. Muñoz, O., Moreno, F., Gómez-Martín, J.C., et al.: Experimental phase function and degree of linear polarization curves of millimetre- sized cosmic dust analogs. *Astrophys. J. Suppl. Ser.* **247**, 19 (2020). <https://doi.org/10.3847/1538-4365/ab6851>
22. Otzuka, T., Nakane, Tomoo: Ultrasonic levitation for liquid droplet. *Japan J Appl Phys* **41**, 3259 (2002). <https://doi.org/10.1143/JJAP.41.3259>
23. Rayleigh, L.: On the pressure of vibrations. *Philos. Mag.* **3**, 338 (1902). <https://doi.org/10.1080/14786440209462769>
24. Trinh, E.H.: Compact acoustic levitation device for studies in fluid dynamics and material science in the laboratory and microgravity. *Rev. Sci. Instrum.* **56**, 2059 (1985). <https://doi.org/10.1063/1.1138419>
25. Vuori, M., Penttilä, A., Muinonen, K., Suhonen, H., Jääskeläinen, J.: Complex refractive index from scattering measurements for an acoustically levitated single particle. *J. Quant. Spectrosc. Radiat. Transf.* **331**, 109269 (2025). <https://doi.org/10.1016/j.jqsrt.2024.109269>
26. Xie, W.J., Cao, C.D., Lü, Y.J., Hong, Z.Y., Wei, B.: Acoustic method for levitation of living animals. *Appl. Phys. Lett.* **89**(21), 214102 (2006). <https://doi.org/10.1063/1.2396893>
27. Yosioka, K., Kawasima, Y.: Acoustic radiation pressure on a compressible sphere. *Acustica* **5**, 167–173 (1955)

Publisher's Note Springer Nature remains neutral with regard to jurisdictional claims in published maps and institutional affiliations.